Photolytic aging of organic aerosol from pyrolyzed urban materials

Katherine S. Hopstock,[1] Alexandra L. Klodt,[1] Qiaorong Xie,[2] Michael A. Alvarado,[1] Alexander Laskin,[2,3] Sergey A. Nizkorodov[1]

[1] Department of Chemistry, University of California, Irvine, Irvine, CA 92697, USA.

[2] Department of Chemistry, Purdue University, West Lafayette, IN 47907, USA.

[3] Department of Earth, Atmospheric and Planetary Sciences, West Lafayette, IN 47907, USA.

* Corresponding author's e-mail: nizkorod@uci.edu

KEYWORDS: wildland-urban interface fire, organic aerosol, pyrolysis, urban materials, polymeric materials, photochemistry

TOG Graphic:

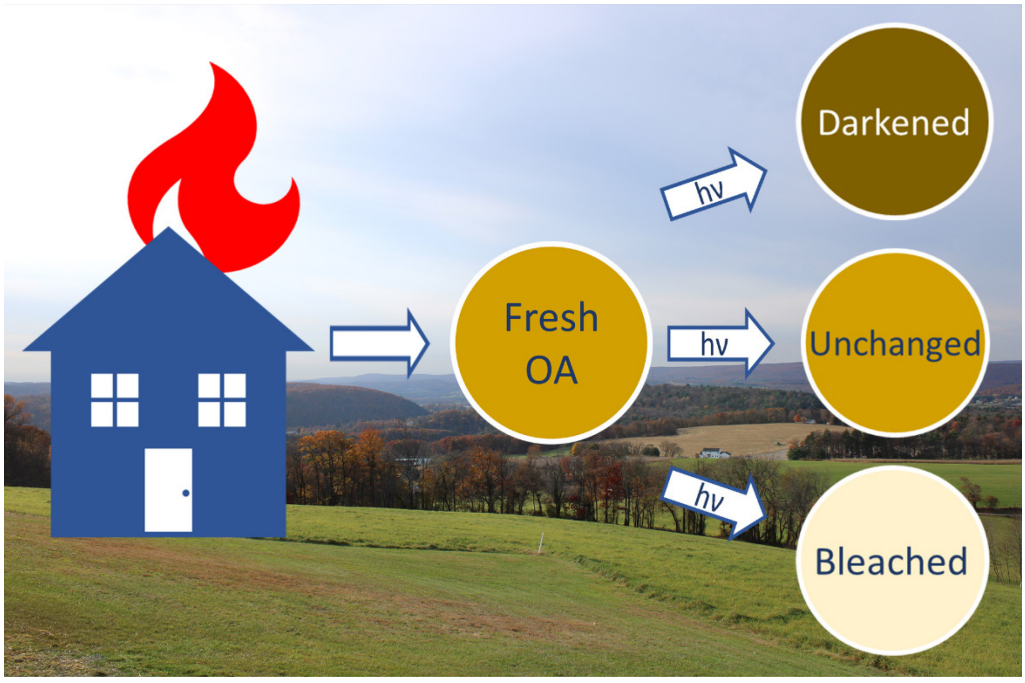

ENVIRONMENTAL SIGNIFICANCE

The frequency of fires occurring at the wildland-urban interface is increasing, with biomass and a wide range of human-engineered materials serving as fuels. Urban material combustion is an important source of atmospheric particulate matter emissions. Smoke particles that can absorb visible solar radiation are especially important because they reduce visibility and lead to atmospheric warming. This work determines the extent to which particulate matter from the burning of different urban materials can absorb sunlight. Additionally, it shows that light-absorbing properties of this particulate matter change upon exposure to solar UV radiation by 1) decomposing light-absorbing compounds (photobleaching) or 2) producing stronger light-absorbing compounds from photooxidation of smaller molecules (photoenhancement). On average, photoenhancement is a more important effect resulting in increasing light absorption by the particulate matter after it travels through the air. This means that smoke particles emitted during wildland-urban interface fires may have a strong effect on visibility and climate.

ABSTRACT

Emissions from large-scale fires significantly contribute to the atmospheric burden of primary organic aerosol (OA). The frequency of fires occurring at the wildland-urban interface (WUI) is increasing, with biomass and a wide range of human-engineered materials serving as fuels. The chemical composition and optical properties of OA from WUI fires are poorly characterized, and this work seeks to understand how direct photolytic aging alters the light absorbing properties of particulate matter generated from WUI fires. Ten flammable urban materials were selected to represent structural and furnishing components commonly combusted in urban fires: electrical 12 AWG wire (white PVC coating), ceiling tile, synthetic fabric, electrical 23 AWG wire (purple PVC coating), lumber, drywall, fiberboard, vinyl flooring, plywood, and carpet. Each material was pyrolyzed at 600 °C under N_2 in a tube furnace and resulting smoke particles were collected on Teflon filters or deposited on fused silica optical windows. OA samples were aged by exposing them to simulated solar radiation (near-UV radiation, 280-400 nm) directly on the collection substrates. Mass absorption coefficients (*MAC*) values and Absorption Angström Exponents (*AAE*) of the unaged and aged OA were calculated from spectrophotometry measurements taken after extracting OA in suitable organic solvents. We observed variable trends

after short-term exposure to UV radiation: six out of ten types of urban OA exhibited photoenhancement, two exhibited photobleaching, and the remaining two experienced negligible change after 2 h of photolytic aging. The average *AAE* value for unaged OA was 8.8 ± 1.3 and decreased to 7.3 ± 0.9 after aging, reflecting increased absorption in the visible range of the spectrum after the UV exposure, and an evolution from very weakly to weakly absorbing brown carbon. Long-term UV exposure results indicate that most photochemical change occurs within the first few hours of irradiation. These results suggest that WUI fires efficiently produce brown carbon, which becomes increasingly light-absorbing in sunlight.

1. INTRODUCTION

Aerosols affect the propagation of radiation through Earth's atmosphere by directly absorbing or scattering incoming solar radiation. Black carbon (BC) and brown carbon (BrC) are components of carbonaceous aerosol particles that absorb solar radiation and contribute to direct forcing on climate by aerosols. BC absorbs strongly over a broad wavelength range and is commonly attributed to soot particles emitted from biomass burning and incomplete combustion of fossil fuels.[1] BrC is characterized by a negligible absorption coefficient at the red edge of the visible spectrum (600-700 nm) and has a much stronger absorption coefficient in the near-UV and blue range of the spectrum (300-500 nm), attributing to its brown color.[2–4] BrC can be emitted from the burning of biomass materials (wildfires,[5–8] domestic wood burning,[9] and cookstove emissions[10]) and its optical properties are highly variable and dependent upon their biofuel source and combustion conditions.[11–13] Atmospheric BrC can also result from the oxidation of aromatic hydrocarbons producing light-absorbing secondary organic aerosol (SOA).

The high chemical reactivity of OA alters its chemical composition and optical properties on atmospherically relevant timescales. Solar radiation drives many of these aging processes by directly photolyzing light-absorbing species, and also through indirect photochemical processes, such as secondary reactions of OA compounds with photochemically produced free radicals and photosensitized reactions.[10,14] Many studies have been conducted to examine the aqueous photochemistry of OA extracts to simulate the photochemical processing of organics dissolved in fog and cloud water.[15–23] Less attention has been given to simulating photochemical processing that occurs inside the organic phase of particles. This organic phase represents a unique environment for photochemistry because of its higher viscosity and reduced polarity compared to an aqueous solution resulting in different photochemical mechanisms in organic particles and in aqueous solutions. Aerosol particles have been estimated to spend 85% of their respective life cycles under non-cloud-activated conditions, thus photochemistry will often take place in the predominantly organic phase.[24] Even under cloud-activated conditions, photochemistry in the organic phase is also important as only a fraction of OA is water soluble.

Previous studies of condensed-phase photochemistry in OA have primarily focused on the photodegradation of SOA particles generated from terpene ozonolysis.[25–27] In this case, mass loss was observed upon UV irradiation of α-pinene and d-limonene ozonolysis SOA,[28–30] which was driven by the direct photolysis of peroxide and carbonyl functionalities as well as secondary

reactions of the resulting free radicals.[28,31–34] A few studies have characterized the mass loss and absorption changes of SOA-containing nitrophenols during UV irradiation.[30,35–37] Additionally, there have been a few studies observing the optical properties of suspended OA produced from burning or pyrolysis, and these generally observe an increase in absorption at long wavelengths with UV irradiation, sometimes followed by photobleaching.[38–40] However, it was difficult to cleanly separate the effects of gas-phase and condensed-phase photochemistry in these experiments.

Even less attention has been given to the photolytic aging of biomass burning organic aerosol (BBOA). Fleming et *al.* (2020) identified major chromophores in BBOA from the combustion of several biofuel types and observed the loss of individual chromophores by utilizing chromatographic separation followed by photodiode array spectrophotometry and high-resolution mass spectrometry.[21] They found that the majority of chromophores were lost after approximately 33 hours of UV irradiation, with the exception of a few photorecalcitrant compounds.[21] To the best of our knowledge, this has been the only study to investigate changes in the optical properties of BBOA particles induced by photolysis in the organic particle phase. It is still unclear how photolytic aging impacts the chemical composition and optical properties of OA generated from biomass combustion. Further, even less is known about the optical properties and photochemical aging of OA generated by fires at the wildland-urban interface (WUI).

The frequency of fires occurring at the WUI is increasing, indicating that the composition and properties of the wildfire related OA are dictated not only by burning biomass but also by the burning of human-engineered materials.[41] The WUI is defined as the area where urban development encroaches upon borders of private and public wildlands.[42] In 2000, 39% of all housing units in the continental United States occupied WUI land.[43] Burke et *al.* (2021) estimated that 50 million homes (and counting) are located in WUI areas in the United States.[44] Climate change has led to more frequent occurrences of large scale forest wildfires that devastatingly destroy urban homes and buildings located at the WUI.[45,46] The effect of urban fire emissions (and its subsequent change) on Earth's radiative forcing is unknown. Blomqvist et *al*. (2007) reported that wood, particleboard, paper, textiles, polyvinyl chloride (PVC), polyurethane, polyethylene, polystyrene, acrylonitrile butadiene styrene, tarred roofing, linoleum, and rubber products were present during building fires in Sweden (1999) that lead to the emissions of volatile organic compounds (VOCs), polycyclic aromatic hydrocarbons (PAHs), and dioxins.[47] Prominent VOCs

related to the burning of urban buildings, farms, and household materials have been previously characterized,[47–49] however, neither the chemical composition nor the aging of this WUI particulate matter have been characterized. This study is the first to conduct photolytic aging experiments using laboratory generated OA representing emissions from WUI fires. Materials representative of engineered wood, plastics, construction materials, textiles, and furnishings were selected to cover the major categories of urban materials combusted in WUI fires.

2. EXPERIMENTAL

Flowcharts of experimental procedures can be found in the Supplemental Information in **Scheme S1** and **Scheme S2**.

2.1 Ten urban materials

Ten samples of flammable urban materials were selected in this study to represent structural and furnishing components present in urban fires: electrical 12 AWG wire (white PVC coating), ceiling tile, fabric, electrical 23 AWG wire (purple PVC coating), lumber, drywall, fiberboard, vinyl flooring, plywood, and industrial carpet. More specific details on the materials can be found in **Table S1**. The 12 AWG wire (white PVC coating) and 23 AWG wire (purple PVC coating) will be referred to as "thick PVC wire" and "thin PVC wire", respectively. All urban materials melt or thermally degrade at temperatures less than that used in our pyrolysis experiments (600 °C).

2.2 Organic aerosol (OA) generation

Experiments were conducted similarly to our previous work on biomass pyrolysis.[50] Pyrolysis is the thermal decomposition of biomass under oxygen limited conditions with temperatures between 300-800 °C.[51] Fires often transition between smoldering (450-700 °C) and flaming (1500-1800 °C) combustion with their genesis process being pyrolysis.[52] Therefore, 600 °C is suitable to mimic real pyrolysis combustion. For each pyrolysis experiment, approximately 200 mg of one tested flammable material (**Table S1)** was placed in a ceramic pyrolysis boat and then inserted into a 2.1 cm I.D. / 2.5 cm O.D. fused silica tube, upstream from the Thermolyne F21135 Tube Furnace (**Scheme S1b**). The tube was sealed and continuously purged with N_2 gas (~0.7 standard liters per minute). A 40 cm section of the tube, downstream from the pyrolysis boat, was heated to 600 °C, and once at this temperature, the tube was pushed inside to bring the urban

material into the heated zone to start the pyrolysis. The starting pressure was ~760 Torr and did not exceed 770 Torr during the experiment. A flow of N_2 gas was constant during pyrolysis and was utilized to push the generated aerosol and fumes through the fused silica tube for collection. The setup was not reopened until collection had ceased. OA sample from each urban material was collected for 10 min starting from the moment the smoke appeared in the flow (**Figure S1**). Samples of tested carpet material were also pyrolyzed at 800 °C and 1000 °C to explore the effects of higher pyrolysis temperatures (**Figure S2**). Pyrolysis experiments at 600 °C produced urban OA that favored BrC production, and all subsequent experiments were done at this temperature.

Samples were collected on two different substrates approximately 1 m downstream from the heated zone, at which point the flow cooled to 42 °C. For most experiments, the collection was done on PTFE 47 mm Teflon filters, which are stable at temperatures less than 350 °C (Millipore Sigma, Fluoropore Membrane Filter, FGLP04700, 47 mm, 0.22 μm pore size) (**Figure S1)**. A subset of samples were collected on optical windows (ISP Optics, Fused Silica IR Grade Windows, QI-W-12-1, 12.7 mm diameter, 1 mm thick) using a single-stage electrostatic precipitator (ESP) (TSI 3089 Nanometer Aerosol Sampler, -5 kV) equipped with a Kr-85 neutralizer (TSI Model 3077 Aerosol Neutralizer). Samples (both Teflon filters and fused silica windows) were weighed after collection using a Sartorius ME5-F microbalance (± 1 μg precision) and the OA mass was calculated. For the samples collected on Teflon filters, the emission factors (EF), defined as the mass of OA collected per urban material mass used in pyrolysis (g kg^{-1}), were calculated from the measured mass collected, assuming that the filters had 100% collection efficiency.

2.3 UV-visible spectroscopy measurements and effects of solvents

After collection, Teflon filters were cut into four equal pieces and each quarter was extracted, separately in 10 mL, using four different solvents: "orgmix" (acetonitrile, dichloromethane, hexane 2:2:1 by volume), methanol, water, and n-octanol. A 2 mL aliquot of each OA extract was transferred into a 1 cm fused silica cuvette and a dual-beam spectrophotometer (Shimadzu UV-2450) was used to take UV/Vis absorption spectra, with the corresponding solvent used as a reference. The best-suited extraction solvent for each OA sample was the one that gave the highest absorbance of the extracted material (**Table S1 and Figure S3**). Wavelength-dependent mass absorption coefficients (*MAC*), in the units of cm^2 g^{-1}, were

calculated from the base-10 absorbance (A_{10}), the estimated concentration of OA extracted in solution, C_{mass} (g cm^{-3}), and path length of the cuvette, b (cm) (**Equation 1**).

$$MAC\ (\lambda) = \frac{A_{10}^{solution}(\lambda) \times \ln(10)}{b \times C_{mass}} \qquad \textbf{Equation (1)}$$

To minimize the effects of small baseline drifts during the measurement, the calculated *MAC* values were corrected by subtracting the average *MAC* between 680 to 700 nm (the absorbance in this wavelength range was generally negligible). Absorption Angström Exponents (*AAE*) were calculated from the slopes of the linear fits applied to the log-log plot of *MAC* (λ) values between 280-480 nm.

2.4 Photolysis experiments

On-filter photolysis experiments were performed as described previously.[37] Briefly, samples were irradiated with near-UV radiation from a Xenon arc lamp (Newport Model 66902) with UVC and visible wavelengths removed using a dichroic mirror, a 295 nm long-pass filter (Schott WG295), and a UV bandpass filter (Schott BG1), leaving the majority of the radiation between 280 and 400 nm. A comparison between our lamp spectrum and ambient solar flux is provided in **Figure S4 and Table S2**. One hour in our photolysis setup is approximately equivalent to 0.7 h under the 2 h average Los Angeles solar flux (average taken for 11 AM to 1 PM on November 9th) as calculated using the "Quick TUV" calculator (Madronich, S. ACOM: Quick TUV, 2019),[53] assuming a photolysis wavelength range of 280 to 400 nm (matching our lamp's radiation). This irradiation time (utilizing 2 h average flux) was chosen to match the rooftop photolysis experiments described below. We note that for photochemical processes that take place inside the particles, photolysis of particles immobilized on an inert substrate (such as fibers of a Teflon filter) should give the same products as photolysis of particles suspended in air as long as particles have access to ambient air. There may be a small enhancement of absorption by particles on the filter due to multiple scattering by the filter fibers and changes in particle shapes,[54,55] which is neglected in our estimation of equivalent UV exposure times.

Filter samples were cut into quarters, and each quarter was weighed to estimate the mass of OA on each quarter (as the OA distribution on the filter was not uniform). For irradiation, one quarter was placed vertically in the path of the near-UV beam, such that the filter surface was uncovered and open to laboratory air (photographs of filters before and after irradiation are

provided in **Table S3**). The quarters not being photolyzed were re-sealed until irradiation. After photolysis, the filter quarter was extracted with methanol, n-octanol, or orgmix (using the previously best determined solvent for that urban material) to take a UV-Vis spectrum (**Figures S5, S6, S7**). Since the UV-Vis sample preparation for the filter samples was destructive, each time point required an entire filter quarter and only four time points were taken per filter. The samples corresponding to 0 h, (unaged), 0.5 h, 1 h, and 2 h of irradiation were chosen as reference time points. *MAC* values were then calculated with **Equation 1**. All *MAC* calculations were performed using the mass of the unaged sample, i.e., assuming no evaporation or other mass loss occurred. Based on previous SOA photolysis experiments, we do expect some mass loss to occur with photolysis,[29,56] so all *MAC* values reported in this work should be considered as lower limits.

For most samples, the extracted filter quarters exhibited the original white color of the Teflon filter, suggesting that all the light-absorbing material was extracted. However, residual OA material was visible on the Teflon filters after photolysis and extraction for three materials: lumber, fabric, and vinyl flooring (**Figure S8**). To remedy this, we collected lumber, fabric, and vinyl flooring OA on fused silica windows to facilitate extraction after photolysis (**Scheme S2**). Similarly to the Teflon filter experiments, samples on fused silica windows were photolyzed for 0.5 h, 1 h, and 2 h. Each photolyzed sample was extracted from the window in the previously determined best solvent, absorption spectra were taken, and spectra from the fused silica window experiments were compared with those of the Teflon experiments (**Figures S9, S10, S11, S12**). Each sample extraction from a fused silica window was destructive, meaning that each time point required the preparation of a new pyrolysis sample.

2.5 High-resolution mass spectrometry experiments

One sample, namely thin PVC wire OA, was selected for bulk compositional analysis using high resolution mass spectrometry (HRMS) to identify the chromophore responsible for the distinct absorption bands in its absorption spectrum. As this was the only material to showcase distinctive absorption band features, only thin PVC wire OA was examined with HRMS in this study. Mass spectra were recorded with a Thermo Scientific Vanquish Horizon ultrahigh pressure liquid chromatograph coupled to a Vanquish Horizon photodiode array spectrophotometer and to a Q Exactive Plus high-resolution mass spectrometer (UHPLC-PDA-HRMS) using heated electrospray ionization in the negative mode (**Figure S13**). More information can be found in **Appendix A** of the Supporting Information.

In additional experiments, portions of selected OA filter samples (carpet, vinyl tile, and fiberboard OA) were loaded individually onto copper pot stubs used in the temperature-programmed desorption – direct analysis in real time – high resolution mass spectrometry (TPD-DART-HRMS) experiments[57] using the Q-Exactive™ HF-X Orbitrap mass spectrometer. Mass spectra were recorded in negative mode, at mass resolving power of m/Δm ~ 240,000 @ 200 m/z and acquisition frequency of 1.5 Hz in the full MS scan mode in the mass range of 100 – 1000 Da (**Figures S14 and S15**). HRMS peak lists were inferred from total ion chromatograms recorded in TPD experiments, integrated over elution times corresponding to selected temperature ranges, and then were background subtracted using the Xcalibur software. Peak lists were extracted with the Decon2LS software and processed using Excel macros developed for *m/z* peak alignment, blank subtraction, and ^{13}C isotope clustering and filtering.[58] The following constraints were applied for all formula assignments: $C_{1\text{-}40}$, $H_{1\text{-}100}$, $O_{1\text{-}25}$, and $N_{0\text{-}3}$, mass tolerance of ± 2.0 ppm. Further details of these experiments, associated data interpretation and data processing can be found elsewhere.[57]

2.6 Additional photolysis experiments

Carpet, vinyl flooring, and fiberboard OA were selected to evaluate how urban OA absorption properties change over longer time scales. Following the same procedures described previously, carpet, vinyl flooring, and fiberboard OA were collected on Teflon filters, cut into four equal fractions, and aged under the Xenon arc lamp. Subsequent extraction and absorption measurements were taken (**Figure S16**). 0 (unaged), 1, 6, and 18 h time points were used for the long-term photolysis.

Drywall OA was selected to compare photolytic exposure from the laboratory photolysis setup (described previously) versus exposure from ambient sunlight. The sample was placed outside on the rooftop of the UC Irvine chemistry building (Rowland Hall) on November 9, 2022 (**Figure S4**). Spectral flux density calculations (**Table S2**) concluded that one hour of exposure under the Xenon arc lamp equated to 0.7 h of sunlight between the hours of greatest solar flux in Irvine, CA (11 AM to 1 PM) on November 9th. Subsequent extraction and absorption measurements were taken and compared with an unaged drywall OA sample (**Figure S17**).

3. RESULTS AND DISCUSSION

3.1 Solubility of tested OA

Ten urban flammable materials (**Table S1**) were pyrolyzed (under N_2) in a tube furnace and resulting OA particles were collected on substrates. **Figure S1** shows representative photographs of resulting filter-collected OA during pyrolysis at 600 °C. The visual appearance of the collected OA varied amongst materials, ranging from gray to light and dark yellow. In addition, carpet OA appearance varied with increasing pyrolysis temperature (**Figure S2**). OA had a brown color resembling that of biomass burning BrC at 600 °C and transformed to OA resembling elemental, black carbon at temperatures exceeding 800 °C. Hence, 600 °C was chosen for all subsequent experiments because samples prepared at > 800 °C could not be efficiently extracted in organic solvents.

Corresponding EFs (**Table S1**) ranged from 1 g kg^{-1} (drywall) to 47 g kg^{-1} (lumber), indicating a wide range in the capacity for producing particulate matter from the selected urban materials. Our EF values are likely underestimated due to particle wall loss in the pyrolysis setup. The generated smoke moved from the heated zone, through the fused silica and Teflon tubing before collection on the filter (**Scheme S1b**), providing plenty of surfaces for the wall loss. Under-ventilated conditions (i.e., smoldering combustion) tend to produce incomplete combustion with enhanced particulate matter production.[59] Because real fires undergo various stages of flaming (well-ventilated conditions) and smoldering (under-ventilated) conditions, our EF values cannot be directly compared with those reported for combustion experiments. With that being said, our wood-based urban materials (lumber and plywood) are well within reported EF ranges for flaming and smoldering combustion.[48]

Methanol extraction, typically the solvent system of choice, is not as effective in BrC extraction from BBOA as methanol/dichloromethane (1:1 and 1:2, *v/v*), tetrahydrofuran, and non-dimethylformamide.[60] Therefore, solvent extractions efficiencies were assessed for all OA samples. The best extraction solvent was determined by the highest overall *MAC* values in **Figure S3** and are listed in **Table S1**. Consistent with prior BBOA extraction studies,[60,61] for all OA samples tested here, water extracted the least OA, as indicated by lower *MAC* values compared to the other solvent systems (**Figure S3**). The samples had comparable solubility in orgmix, methanol, and octanol. With the notable exception of the thin PVC wire, the *MAC* spectra in all organic solvents had the same shape, suggesting near complete extraction of all material from the filter.

3.2 Unaged urban OA absorption spectra characteristics

Because BrC is a complex mixture of individual chromophores, the absorption spectra of ambient BrC are typically featureless, with the absorption coefficient smoothly increasing from visible to UV wavelengths.[2] The absorption coefficient of BrC often scales with wavelength and a power law, $\propto \lambda^{-AAE}$, where *AAE* stands for Absorption Angström Exponent. For ambient BrC, *AAE* varies from 2 to 11, depending on the OA composition.[2,62,63] **Figure 1a** shows the *MAC (λ)* values of all unaged OA samples extracted in the best-suited solvent. All ten OA absorb strongly at shorter wavelengths (UV) and have weak absorption over the visible range, characteristic of BrC.[2] Most OA have a slight absorption band at ~250 nm, attributed to a π to π* transition of conjugated/aromatic organic compounds.[39,64,65] The resulting *AAE* values ranged from 6.0 to 11.6 with the average being 8.8 ± 1.3 (value ± standard deviation). These values fall within expected *AAE* values for BrC previously reported for SOA BrC and BBOA BrC.[2,62,63]

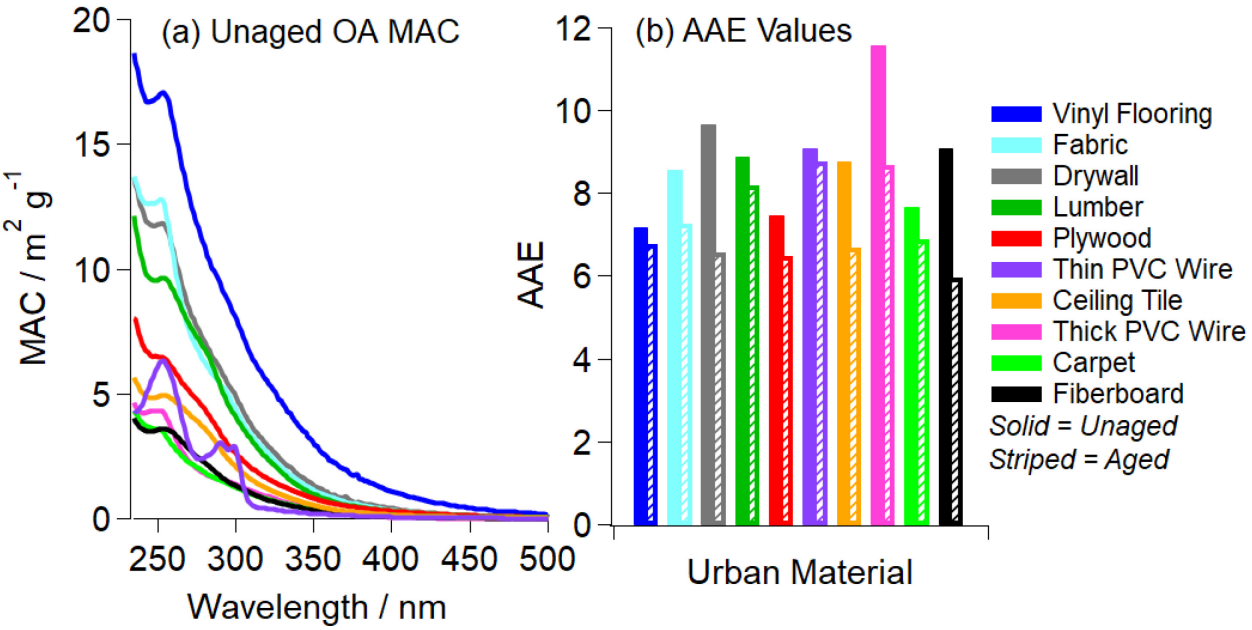

Figure 1. Panel (a) shows the wavelength-dependent mass absorption coefficient (*MAC*) values recorded after pyrolysis of urban materials and extraction in the best-suited organic solvent (**Table S1**). *MAC* values were calculated assuming 100% extraction efficiency from the Teflon filter. Boxcar averaging of the *MAC* data (over a 5 nm range) was utilized to improve signal-to-noise ratio. Panel (b) shows the *AAE* values for unaged OA (solid bars) and 2 h aged OA (striped bars). The effective *AAE* values were obtained from the linear fits of log(*MAC*) vs. log(λ) data in **Figure S5** in the 280-480 nm range.

3.3 Transformations of OA absorption caused by photolysis

Three distinct color changes of the OA samples were observed: photoenhancement (samples became visibly darker in color), photobleaching (samples became lighter in color), and unchanged (no perceptible color change was observed). These qualitative visual observations were confirmed by the UV-Vis spectroscopy measurements that were taken after extracting OA at each irradiation time point.

Figure 2 shows the *MAC* values for two OA samples generated from the pyrolysis of drywall (**Figures 2a and 2b**) and thin PVC wire (**Figures 2c and 2d**). The subplots in each panel show the *MAC* values integrated over their respective wavelength range (280 to 400 nm for the near-UV and 400 to 700 nm for the visible range), normalized to their corresponding unaged *MAC* values. Both drywall OA and thin PVC wire OA show a similar decrease in the UV range integrated *MAC* (**Figures 2a and 2c**), but different trends were observed in the visible range. There was an increase by a factor of 2.75 (relative to the unaged value) for the drywall OA visible integrated *MAC* (**Figure 2b**), whereas thin PVC wire OA experienced a decrease by a factor of 1.21 compared to the unaged sample (**Figure 2d**). These results confirmed visual observations that photoenhancement in the absorption coefficient occurred for drywall OA and photobleaching occurred for thin PVC wire OA (**Table S3**). Similar to the results in **Figure 2**, **Figure S6** shows that fiberboard OA exhibited photoenhancement (increase by a factor of 3) and carpet OA exhibited photobleaching (2 h aged sample was factor of 1.5 lower than unaged sample). In addition, three other OA samples (thick PVC wire, ceiling tile, and plywood) exhibited photoenhancement effects in the visible range (increase by factors of 1.8, 1.6, and 1.5, respectively, compared to the unaged value) upon 2 h of direct photolytic aging (**Figure S7**).

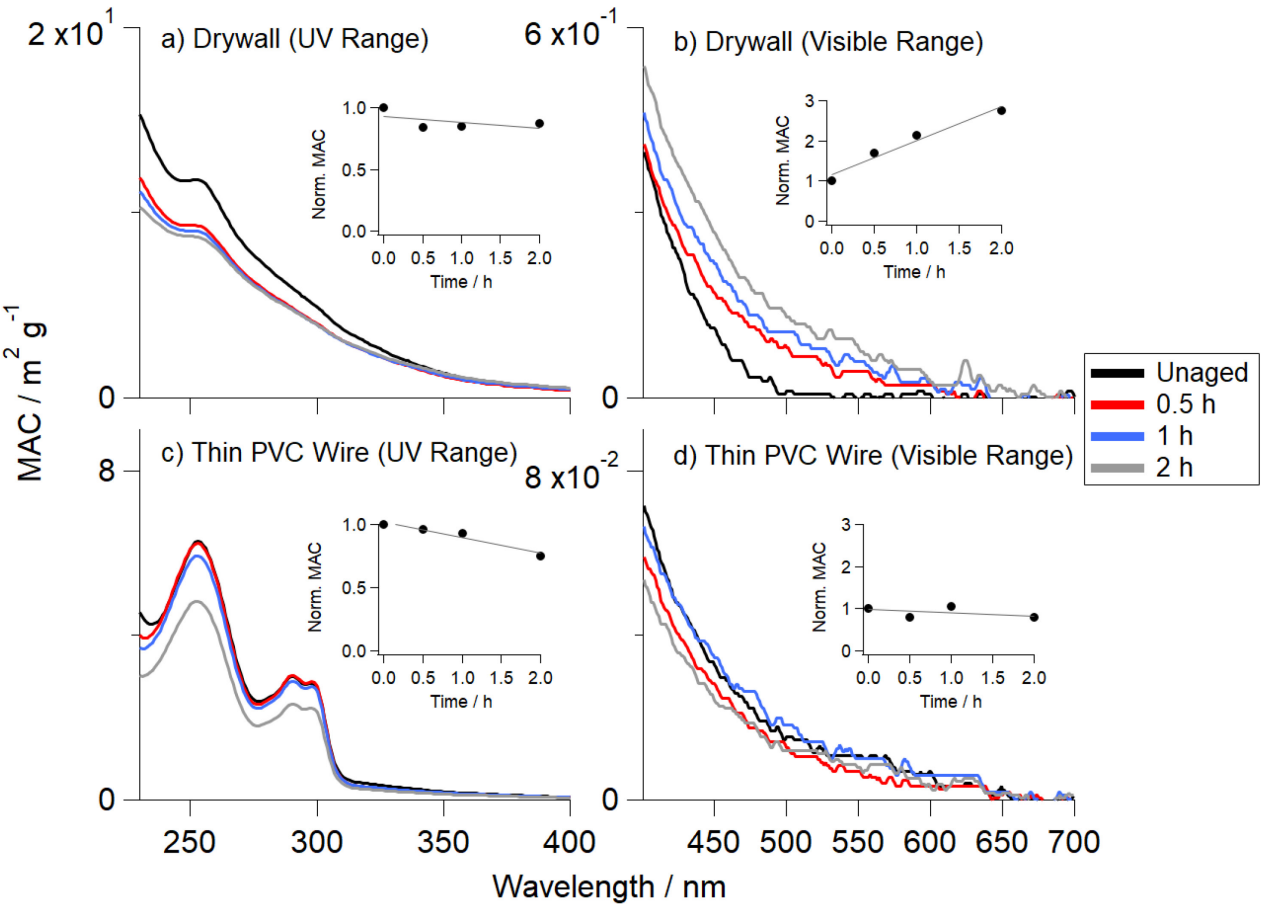

Figure 2. Wavelength-dependent *MAC* values recorded after photolysis on Teflon filters and the subsequent extractions of drywall OA (a and b) and thin PVC wire OA (c and d). Each quarter of the filter was aged separately for 0.5 h (red), 1 h (blue), or 2 h (gray) and is compared with the unaged (0 h) fraction (black). The integrated *MAC* values (normalized to the unaged value) are shown as a subplot in each panel, with the UV integrated over 280-400 nm and the visible integrated over 400-700 nm. Boxcar averaging of the *MAC* data (over a 5 nm range) was utilized to improve signal-to-noise ratio.

The UV exposure not only changed the color of the filters but, in some cases, appeared to affect the solubility of the residual material. Specifically, lumber, fabric, and vinyl flooring OA could not be fully extracted from the Teflon filters after the irradiation (**Figure S8**). This complicated classification of the irradiation effects into categories of photoenhancement or photobleaching. For example, lumber OA results show a decrease in integrated MAC value by a factor of 1.02 in the visible range Teflon filter experiments (**Figure S9b**), but this result

contradicted the obvious filter darkening observed visually (**Table S3**). To resolve this issue, photolysis experiments for these materials were repeated using OA collected on fused silica windows after passing through an ESP (-5 kV). This collection method allowed for a more complete extraction of lumber, fabric, and vinyl flooring OA post-photolysis (**Scheme S2**). While the Teflon filters collected particles >0.22 μm, the collection by ESP favored smaller particle sizes.[66,67] To this end, composition of smaller particles may have enhanced the solubility of photolyzed OA. ESP experiments for lumber OA exhibited an increase in the UV by a factor of 4 and an increase in the visible by a factor of 5.5 (**Figure S9c and S9d**) indicating that the residual OA prevented the full representation of light-absorptive properties of the sample after photolytic aging. Fabric and vinyl flooring OA exhibited no net change (0.9 > ratio (2 h aged to unaged) < 1.1) in both the Teflon and fused silica window experiments (**Figures S10 and S11**).

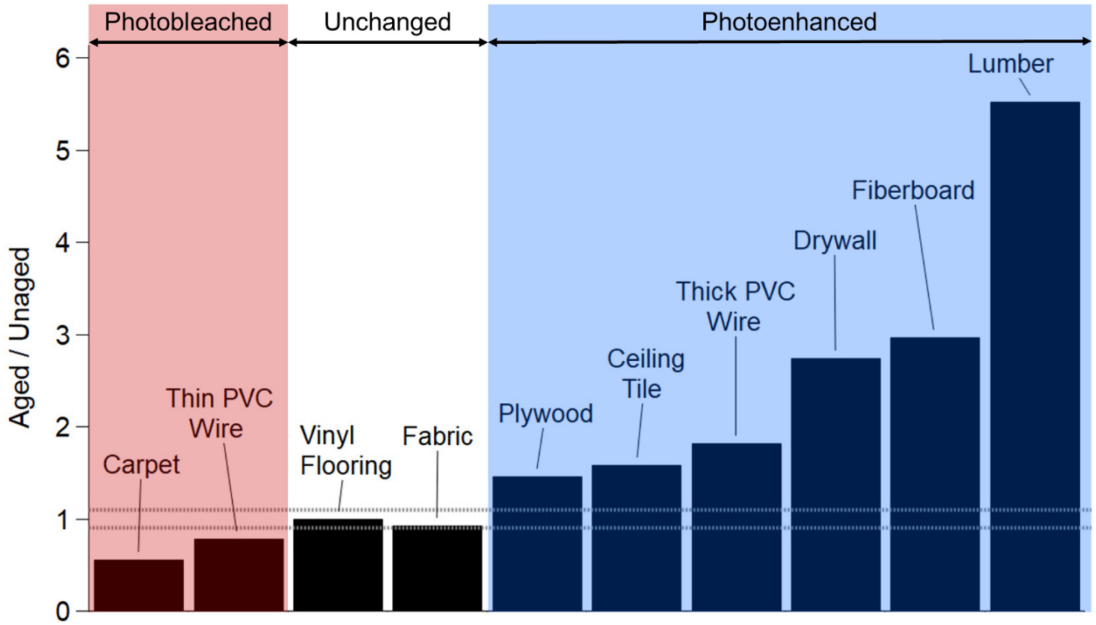

Figure 3. Ratios of the 2 h aged to unaged integrated, visible range *MAC* values. The reported ratios were calculated by integrating the *MAC* values in the visible range (400-700 nm) then referencing the 2 h aged, integrated *MAC* value to that of the unaged, integrated *MAC* value. The shading color corresponds to classification of OA into three categories: photobleached (red), unchanged (white) and photoenhanced (blue). The dashed line (0.9 to 1.1) indicates the threshold for the unchanged category.

Figure 3 presents the ratios of 2 h aged to unaged *MAC* values integrated over the visible range for all 10 urban materials. As mentioned above, three types of trends were observed over the 2 h aging time: photobleached, unchanged, and photoenhanced. In addition to these results in the visible range, **Figure S12** shows that all but one OA sample (lumber) decreased in UV range *MAC* values after 2 h of photo-aging, as indicated by ratio greater than 1.1. Carpet OA and thin PVC wire OA (red region in **Figure 3**) photobleached upon UV exposure, indicating chromophore fragmentation occurred more efficiently than chromophore formation. Similar results were observed by Ye et *al.* (2019) as they studied the aqueous-phase photochemical oxidation of a model BBOA compound, 4-ethylphenol.[68] They observed degradation and fragmentation upon initial exposure to hydroxyl radical oxidation under UV light.[68] Since we conducted photolytic aging experiments without intentionally added OH radical sources, we hypothesize that the observed photobleaching effects were a result of UV light induced OH radical production, leading to the degradation of chromophoric species in carpet OA and thin PVC wire OA.

Six urban materials (blue region in **Figure 3**) exhibited photoenhancement. We hypothesize that photochemically-driven formation of stronger chromophores occurred by free radical (OH). and triplet-excited state reactions occurring in the OA material. Such reactions have been shown to lead to the formation of chromophores in aqueous photochemistry,[69–72] but they have also been reported to occur in model OA material.[35,36] More specifically for model BBOA chromophores, Hems and Abbatt (2018) observed absorbance enhancement in the visible wavelength range for nitrocatechol, nitroguaiacol, and dinitrophenol due to the formation of functionalized products after exposure to a steady state concentration of OH radical.[73] These studies proved that OH radical oxidation of dissolved BBOA compounds can lead to functionalized and oligomerized products with enhanced absorption in visible wavelengths.

Fabric OA and vinyl flooring OA *MAC* values (white region in **Figure 3**) exhibited ratios greater than 0.9 but less than 1.1 when 2 h aged measurements were referenced to the unaged (**Figure S10 and S11,** respectively). Noticeably for these two materials, photoenhancement occurred in the first hour of aging then photodegradation occurred between 1 and 2 h of aging, thus returning the *MAC* back to the initial unaged value. Previous studies investigating BrC photolytic aging have observed similar trends. Secondary BrC has been observed to rapidly photobleach,[74] whereas primary BrC from biomass burning has been observed to undergo both photoenhancement and photobleaching during the course of UV exposure, with initial

photoenhancement followed by photobleaching.[22,38,39] Aqueous-phase UV/OH radical exposure studies showed that product formation occurred during oxidation of organic compounds and initial increases in absorption are attributed to functionalization of chromophores.[16,22,73] Over time, loss of absorption occurs when further reactivity leads to fragmentation.[16,22,73,75] We observe this "dynamic" nature in the fabric OA and vinyl flooring OA cases. Further mass spectrometry analysis (at each irradiation time point) is necessary to determine the mechanism(s) of evolution.

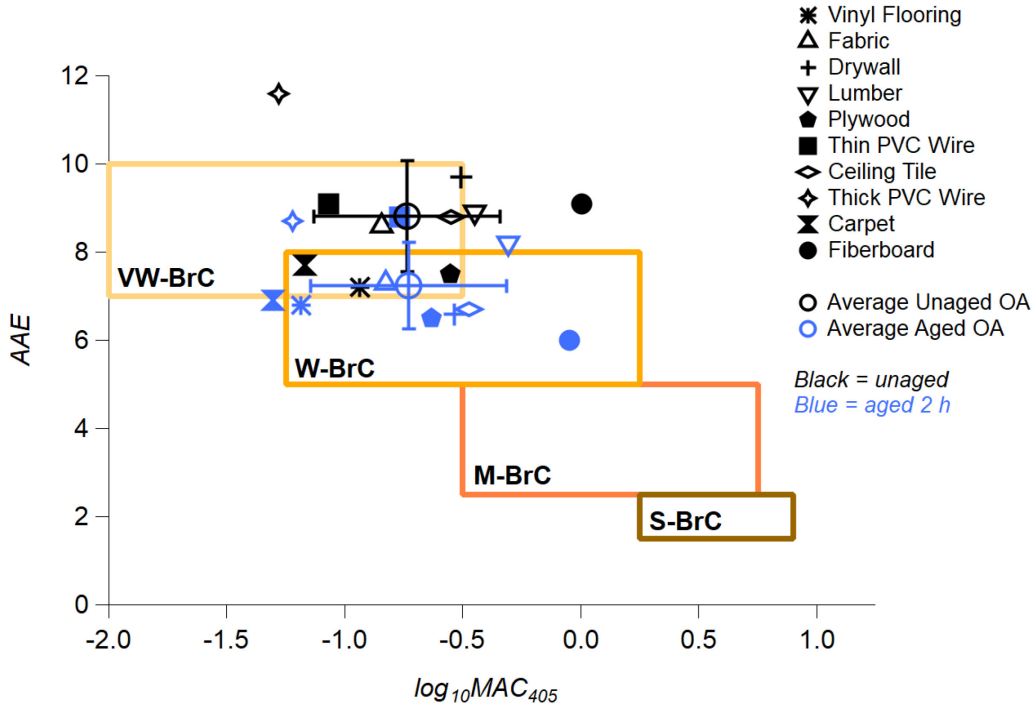

Figure 4. Urban OA BrC optical properties mapped in *AAE-log*$_{10}$ *vs. MAC*$_{405}$ space following the classification introduced by Saleh (2020) and further adapted by Hettiyadura et *al.* (2021).[62,76] Boxed areas represent very weakly (VW), weakly (W), moderately (M), and strongly (S) absorbing BrC classes. The markers correspond to the values of *AAE* calculated for a wavelength range of 280-480 nm for unaged urban OA (black markers) and the 2 h aged urban OA (blue markers). The global average, unaged OA (black open circle) and average, 2 h aged OA (blue open circle) are shown to illustrate a change upon photolytic aging.

All *MAC* and *AAE* values for the OA samples unaged (0 h) and after 2 h of photolysis (**Figure 1** and **Figure S5**) are incorporated in **Figure 4**. The *MAC*$_{405}$ of unaged OA (black markers) are compared to OA aged for 2 h (blue markers), placed into the context of the optically based BrC absorption strength classification introduced by Saleh (2020) and modified by Hettiyadura *et al.*

(2021).[62,76] Note that these *MAC* values were calculated using the mass of the unaged sample, and some mass loss is expected with photolysis. Therefore, reported *MAC* values are likely to be underestimations of the true *MAC* values post-photolysis. Upon photolysis, there is a downward shift in *AAE* values from VW → W BrC. These results are similar to those reported in Hettiyadura *et al.* (2021) for fresh biomass burning BrC and biomass burning BrC that darkened with NO_3 chemistry.[76] The average *AAE* value for all ten urban OA after photolyzing for 2 h reduced from 8.8 ± 1.3 to 7.3 ± 0.9. All materials experienced a reduction in *AAE* value upon short term aging, as indicated by striped bars in **Figure 1b**. As we are examining components commonly combusted in fires at the WUI, the average *AAE* shift shown in **Figure 4** reflects that WUI OA exhibits an overall absorption enhancement effect with UV aging.

3.4 Compositional results of unaged and aged OA

Thin PVC wire OA is an anomaly in this data set in two ways. First, the two types of PVC wire OA (thin and thick) exhibited opposite trends: OA from thin PVC wire (purple) photobleached, whereas OA from thick PVC wire (white) photoenhanced after UV exposure. Second, thin PVC wire OA was the only material to exhibit distinct absorption bands, one at 253 nm and a doublet at 290 nm and 300 nm (**Figure 1**). Through UHPLC-PDA-HRMS analysis (**Figure S13** and **Appendix A**), we sought to identify the chromophore responsible for these spectral features. While we could not identify the specific chromophore whose absorption would match the distinct doublet at 290+300 nm, we were able to identify phthalic acid as a major contributor to the sample's overall light absorption. Phthalic acid is used in the production of PVC plasticizer, polyester resin, and dyes and is a derivative of phthalic anhydride, a common chemical intermediate in plastic production.[77] Since the thin PVC wire material tested in this study was purple, it is reasonable to suspect that phthalic acid was added alongside a purple dye into the PVC coating. It is possible that the photobleaching effect exhibited by thin PVC wire OA is due to degradation of the phthalic acid chromophore by continued OH radical generation and aging.[75] This (and other trends) will need to be systematically explored in future works with mass spectrometry analysis of all urban OA samples.

To further assess the corresponding changes in chemical composition of OA samples after direct photolysis, we conducted TPD-DART-HRMS experiments to detect chemical transformations in three selected OA samples representative of photobleached (carpet),

photoenhanced (fiberboard) and unchanged (vinyl tile) cases observed in our study (**Figure 3**). The reconstructed HRMS plots of all detected organic compounds in both unaged and aged aerosols are exhibited in **Figures S14** and **S15**. There were 1698/1479 (carpet), 633/379 (vinyl tile), and 956/988 (fiberboard) compounds detected in each of the unaged/aged pairs of OA samples, respectively (**Figure S14**). In each of the pairs, compounds that were affected by the photolysis experiments were selected based on the following criteria: 1) components unique to unaged or aged OA samples and 2) components that decreased or increased by >10% in the aged OA samples. There were 1036/871 (carpet), 470/206 (vinyl tile) and 185/205 (fiberboard) components that satisfied these criteria. The reconstructed HRMS plots summarizing these photolysis-affected compounds are shown in **Figure S15** and the corresponding DBE (double bond equivalent) values versus C (number of carbon atoms) plots are shown in **Figure 5**.

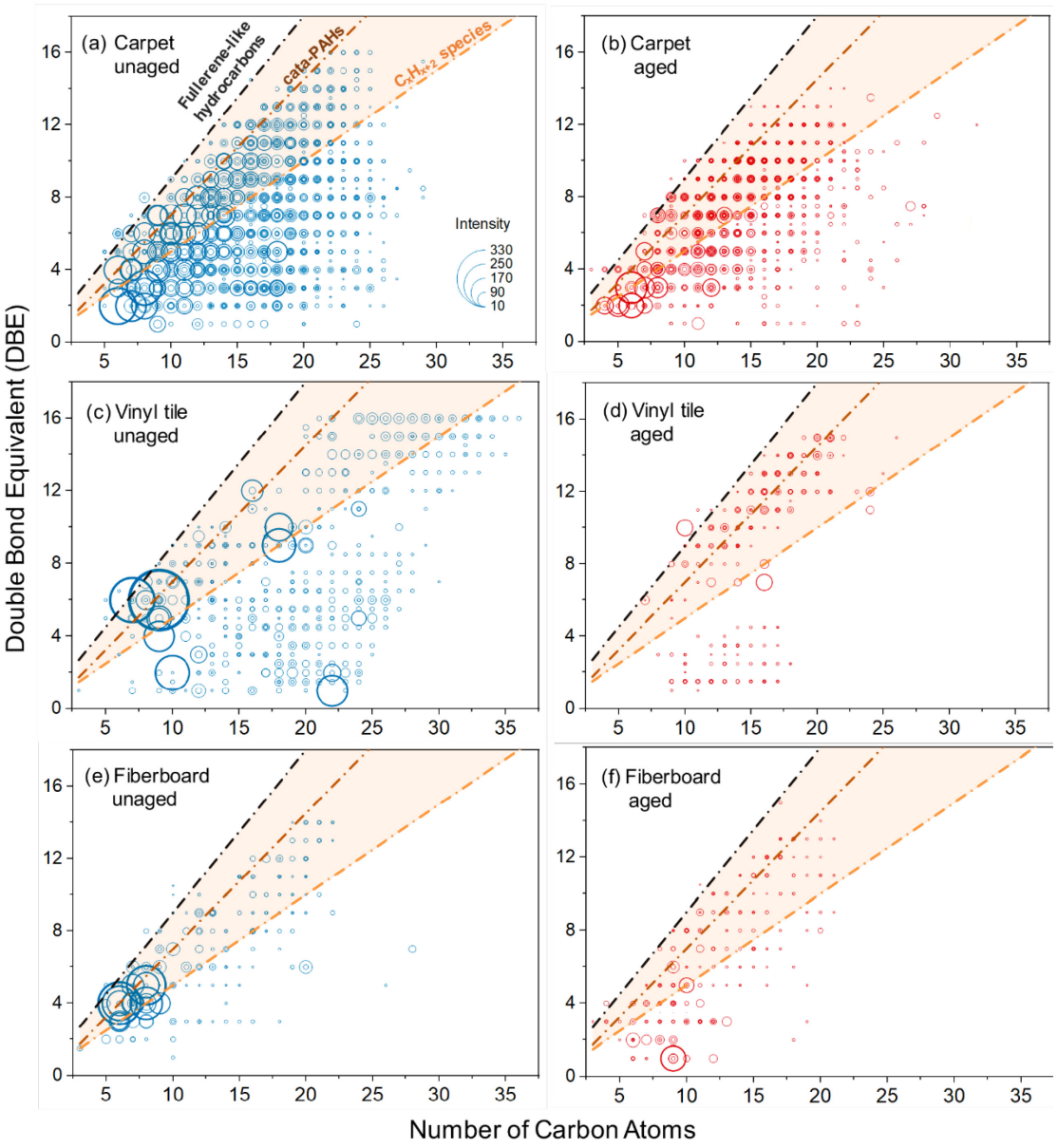

Figure 5. The double bond equivalent (*DBE*) values vs number of carbon atoms corresponding to *the OA components affected by the photolysis reactions (i.e., those that exhibited a >10% change in relative abundance)* detected in unaged (left panels) and aged (right panels) OA samples collected from pyrolysis of carpet (a-b), vinyl tile (c-d), and fiberboard (e-f) samples. Lines indicate DBE reference values of linear conjugated polyenes C_xH_{x+2} (orange line), cata-condensed PAHs (brown line), and fullerene-like hydrocarbons with DBE = 0.9 × C (black line).[78] Data points inside the orange shaded area are potential BrC chromophores. Sizes of the individual points are arbitrarily scaled to the cubic root of the corresponding MS peaks intensities. Occasional

datapoints located above the 0.9×C limiting line correspond to highly aromatic N-containing species.

Because efficient absorption of visible light by organic molecules requires uninterrupted conjugation of π-bonds across significant parts of their carbon skeleton, compounds with DBE/C ratio greater than that of polyenes are potential BrC chromophores,[79] which are located in the plots within shaded areas (**Figure 5**). Qualitative assessment of the BrC chromophore transformations after photolysis can be inferred from visual comparison of **Figure 5 and S15** featuring differences between aged and unaged OA samples. Aged carpet, vinyl flooring, and fiberboard peaks changed by 59 %, 54 %, and 21 %, respectively, compared to the unaged peaks. For the photobleached OA sample (carpet), both the number and intensity of BrC chromophores decreased significantly after photolysis, which is consistent with the observed and commonly expected photobleaching effect. However, more complex compositional changes are observed for the photoenhanced (fiberboard) and unchanged (vinyl tile) OA samples. In both cases, there are relatively small $C_{6\text{-}9}$ BrC compounds with high intensity present in unaged samples, which largely disappear from the aged samples. On the other hand, formation of highly aromatic BrC chromophores of larger $C_{12\text{-}18}$ molecular sizes is clearly observed in the corresponding aged samples. This trend can be plausibly explained by the photochemically induced oligomerization reactions that consume $C_{6\text{-}9}$ monomers and form $C_{12\text{-}18}$ dimer BrC products with stronger absorption properties. In both cases (fiberboard and vinyl tile OA), the overall transformation of the BrC light absorption by the aged OA samples is a combined effect of the degradation of small chromophores and the buildup of the larger chromophores. Depending on the chromophore-specific light absorbing properties, the integrated BrC absorbance of the decayed and the newly formed chromophores may show either null (vinyl tile OA) or photoenhanced (fiberboard OA) effects. These observations demonstrate that urban material BrC pyrolysis products undergo complex reaction chemistry which modifies composition of various BrC chromophores but, simultaneously, their integrated optical properties show no detectable change.

3.5 Additional direct photolysis experiments

Considering the lifetime of an aerosol in the lower atmosphere is not limited to a few hours, we performed additional experiments at longer time scales to see if the trends observed over our 2 h period would continue over longer times. To this end, one OA from each result category

(photobleached, unchanged, and photoenhanced) was photolyzed for up to 18 hours (**Figure S16**). For our photobleaching material (carpet) and our unchanged material (vinyl flooring) the trends over the 18 h time scale matched those in the 2 h time scale. The visible region of the carpet OA continued to photobleach between 1 and 6 h of irradiation but the visible region of the vinyl flooring OA exhibited negligible change over the 18 h of photolysis. For both OA, the most change happened in the first 6 hours of irradiation, producing products that were no longer photochemically active.

In the case of the fiberboard OA (**Figure S16e and S16f**), which photoenhanced during short-term irradiation, photobleaching was observed over longer time scales. It appears that this type of OA first increases in visible absorbance and then ultimately bleaches with continued photolysis. This trend mirrors work done on heterogeneous OH oxidation of particulate BrC,[80] aqueous phase photo-oxidation of biomass burning BrC,[16,23] and photolysis of aqueous biomass burning BrC.[15,16] In the case of primary BrC generated from smoldering pine wood, heterogeneous OH oxidation resulted in absorption enhancement over the first 2.5 h (followed by photobleaching),[80] which is similar to the timeframe observed here. Once again, chromophore build up may be attributed to increased oxidation through OH reactions or oligomerization through either OH or triplet excited state reactions.[3,81] Future work will implement mass spectrometry to identify whether the optical changes seen in this work are attributed to OH functionalization reactions or oligomerization processes.

The experiments described above relied on the filtered Xe-lamp source for driving photochemistry in the OA material. To demonstrate that actual sunlight produces similar results, we selected drywall OA, a material that exhibited significant change with photolysis, and exposed a portion of the filter to direct sunlight and another portion to flux from our photolysis set-up (**Figure S17**). As 1 h under our lamp was estimated to be equivalent to 0.7 h in direct sunlight, the filter portion was exposed to the lamp for 2 h and the other portion was exposed to outside sunlight for 1.4 h. Integration of the UV portion of the *MAC* (280 to 400 nm) shows that the two filter portions exhibited similar degrees of change, within 5 % (**Figure S17**).

4. CONCLUSIONS AND FUTURE WORK

This work explored the optical properties of OA produced from the smoldering pyrolysis of flammable urban materials and their transformations during exposure to solar UV radiation.

Atmospheric aging of OA (via direct photolysis) altered the optical properties of this BrC by 1) decomposing BrC chromophores (photobleaching) or 2) producing stronger chromophores from photooxidation of smaller molecules (photoenhancement).[15,22,23] Plywood, ceiling tile, thick PVC coated wire, drywall, fiberboard, and lumber OA samples exhibited photoenhancement effects, whereas carpet and thin PVC coated wire OA exhibited photobleaching effects with exposure to UV light. Vinyl flooring and fabric OA remained unchanged after photolytic aging. We have observed that, on average, OA from the WUI exhibits increased absorption after the UV exposure. This means that BrC from WUI fires may have stronger effect on visibility and radiative forcing as it undergoes aging in the atmosphere.

Previous work investigated the photolysis of BBOA between 0 to 16 h of irradiation and determined that photobleaching is slow due to competing aging mechanisms by heterogeneous OH oxidation.[21] Photolytic aging of BrC from BBOA has also been seen to have significant OH concentrations in OA extracts when no additional OH source was added.[16] In the present study, we observed significant absorption enhancement of OA from the WUI over the first few hours of photolysis, indirectly suggesting that OH (and likely other free radicals) are produced in the organic phase of the particles during irradiation. To understand the chemical changes responsible for our optical observations, identification and structural characterization of WUI BrC chromophores (before and after photolysis) are needed to determine the mechanism in which this OA transforms and identify if it evolves similarly to BrC from BBOA.

AUTHOR INFORMATION

Corresponding Author

* E-mail: nizkorod@uci.edu

ORCID

Katherine S. Hopstock: 0000-0001-9141-8899

Alexandra L. Klodt: 0000-0002-3558-972X

Qiaorong Xie: 0000-0002-9391-624X

Alexander Laskin: 0000-0002-7836-8417

Sergey A. Nizkorodov: 0000-0003-0891-0052

Author Contributions

K. S. H., A. L. K., and M. A. A. conducted pyrolysis and photolysis experiments. Q. X. conducted experiments and write up of TPD-DART-HRMS results. K. S. H. conducted UHPLC-PDA-HRMS experiments, data analysis, and wrote the manuscript. A. L. K. assisted in manuscript writing. S. A. N. and A. L. designed the experiments, assisted in interpretation of results, and manuscript co-editing.

ACKNOWLEDGEMENTS

This study was supported by the National Oceanic and Atmospheric Administration grants NA22OAR4310196 (University of California, Irvine) and NA22OAR4310195 (Purdue University). The photolysis experiments were done with support from National Science Foundation grant NSF AGS-1853639 (University of California, Irvine).

REFERENCES

(1) Bond, T. C.; Doherty, S. J.; Fahey, D. W.; Forster, P. M.; Berntsen, T.; DeAngelo, B. J.; Flanner, M. G.; Ghan, S.; Kärcher, B.; Koch, D.; Kinne, S.; Kondo, Y.; Quinn, P. K.; Sarofim, M. C.; Schultz, M. G.; Schulz, M.; Venkataraman, C.; Zhang, H.; Zhang, S.; Bellouin, N.; Guttikunda, S. K.; Hopke, P. K.; Jacobson, M. Z.; Kaiser, J. W.; Klimont, Z.; Lohmann, U.; Schwarz, J. P.; Shindell, D.; Storelvmo, T.; Warren, S. G.; Zender, C. S. Bounding the Role of Black Carbon in the Climate System: A Scientific Assessment. *Journal of Geophysical Research: Atmospheres* **2013**, *118* (11), 5380–5552. https://doi.org/10.1002/jgrd.50171.

(2) Laskin, A.; Laskin, J.; Nizkorodov, S. A. Chemistry of Atmospheric Brown Carbon. *Chem. Rev.* **2015**, *115* (10), 4335–4382. https://doi.org/10.1021/cr5006167.

(3) Hems, R. F.; Schnitzler, E. G.; Liu-Kang, C.; Cappa, C. D.; Abbatt, J. P. D. Aging of Atmospheric Brown Carbon Aerosol. *ACS Earth Space Chem.* **2021**, *5* (4), 722–748. https://doi.org/10.1021/acsearthspacechem.0c00346.

(4) Andreae, M. O.; Gelencser, A. Black Carbon or Brown Carbon? The Nature of Light-Absorbing Carbonaceous Aerosols. *Atmos. Chem. Phys.* **2006**, 18.

(5) Washenfelder, R. A.; Attwood, A. R.; Brock, C. A.; Guo, H.; Xu, L.; Weber, R. J.; Ng, N. L.; Allen, H. M.; Ayres, B. R.; Baumann, K.; Cohen, R. C.; Draper, D. C.; Duffey, K. C.; Edgerton, E.; Fry, J. L.; Hu, W. W.; Jimenez, J. L.; Palm, B. B.; Romer, P.; Stone, E. A.; Wooldridge, P. J.; Brown, S. S. Biomass Burning Dominates Brown Carbon Absorption in the Rural Southeastern United States. *Geophysical Research Letters* **2015**, *42* (2), 653–664. https://doi.org/10.1002/2014GL062444.

(6) Ramanathan, V.; Li, F.; Ramana, M. V.; Praveen, P. S.; Kim, D.; Corrigan, C. E.; Nguyen, H.; Stone, E. A.; Schauer, J. J.; Carmichael, G. R.; Adhikary, B.; Yoon, S. C. Atmospheric Brown Clouds: Hemispherical and Regional Variations in Long-Range Transport, Absorption, and

Radiative Forcing. *Journal of Geophysical Research: Atmospheres* **2007**, *112* (D22). https://doi.org/10.1029/2006JD008124.
(7) Lin, P.; Bluvshtein, N.; Rudich, Y.; Nizkorodov, S. A.; Laskin, J.; Laskin, A. Molecular Chemistry of Atmospheric Brown Carbon Inferred from a Nationwide Biomass Burning Event. *Environ. Sci. Technol.* **2017**, *51* (20), 11561–11570. https://doi.org/10.1021/acs.est.7b02276.
(8) Chen, Y.; Bond, T. C. Light Absorption by Organic Carbon from Wood Combustion. *Atmospheric Chemistry and Physics* **2010**, *10* (4), 1773–1787. https://doi.org/10.5194/acp-10-1773-2010.
(9) Budisulistiorini, S. H.; Riva, M.; Williams, M.; Chen, J.; Itoh, M.; Surratt, J. D.; Kuwata, M. Light-Absorbing Brown Carbon Aerosol Constituents from Combustion of Indonesian Peat and Biomass. *Environ. Sci. Technol.* **2017**, *51* (8), 4415–4423. https://doi.org/10.1021/acs.est.7b00397.
(10) Fleming, L. T.; Lin, P.; Laskin, A.; Laskin, J.; Weltman, R.; Edwards, R. D.; Arora, N. K.; Yadav, A.; Meinardi, S.; Blake, D. R.; Pillarisetti, A.; Smith, K. R.; Nizkorodov, S. A. Molecular Composition of Particulate Matter Emissions from Dung and Brushwood Burning Household Cookstoves in Haryana, India. *Atmos. Chem. Phys.* **2018**, *18* (4), 2461–2480. https://doi.org/10.5194/acp-18-2461-2018.
(11) Kirchstetter, T. W.; Novakov, T.; Hobbs, P. V. Evidence That the Spectral Dependence of Light Absorption by Aerosols Is Affected by Organic Carbon. *Journal of Geophysical Research: Atmospheres* **2004**, *109* (D21). https://doi.org/10.1029/2004JD004999.
(12) Rizzo, L. V.; Correia, A. L.; Artaxo, P.; Procópio, A. S.; Andreae, M. O. Spectral Dependence of Aerosol Light Absorption over the Amazon Basin. *Atmos. Chem. Phys.* **2011**, *11* (17), 8899–8912. https://doi.org/10.5194/acp-11-8899-2011.
(13) Zhang, X.; Lin, Y.-H.; Surratt, J. D.; Weber, R. J. Sources, Composition and Absorption Ångström Exponent of Light-Absorbing Organic Components in Aerosol Extracts from the Los Angeles Basin. *Environ. Sci. Technol.* **2013**, *47* (8), 3685–3693. https://doi.org/10.1021/es305047b.
(14) Corral Arroyo, P.; Bartels-Rausch, T.; Alpert, P. A.; Dumas, S.; Perrier, S.; George, C.; Ammann, M. Particle-Phase Photosensitized Radical Production and Aerosol Aging. *Environ. Sci. Technol.* **2018**, *52* (14), 7680–7688. https://doi.org/10.1021/acs.est.8b00329.
(15) Wong, J. P. S.; Nenes, A.; Weber, R. J. Changes in Light Absorptivity of Molecular Weight Separated Brown Carbon Due to Photolytic Aging. *Environ. Sci. Technol.* **2017**, *51* (15), 8414–8421. https://doi.org/10.1021/acs.est.7b01739.
(16) Wong, J. P. S.; Tsagkaraki, M.; Tsiodra, I.; Mihalopoulos, N.; Violaki, K.; Kanakidou, M.; Sciare, J.; Nenes, A.; Weber, R. J. Atmospheric Evolution of Molecular-Weight-Separated Brown Carbon from Biomass Burning. *Atmospheric Chemistry and Physics* **2019**, *19* (11), 7319–7334. https://doi.org/10.5194/acp-19-7319-2019.
(17) Lin, P.; Aiona, P. K.; Li, Y.; Shiraiwa, M.; Laskin, J.; Nizkorodov, S. A.; Laskin, A. Molecular Characterization of Brown Carbon in Biomass Burning Aerosol Particles. *Environ. Sci. Technol.* **2016**, *50* (21), 11815–11824. https://doi.org/10.1021/acs.est.6b03024.
(18) Aiona, P. K.; Luek, J. L.; Timko, S. A.; Powers, L. C.; Gonsior, M.; Nizkorodov, S. A. Effect of Photolysis on Absorption and Fluorescence Spectra of Light-Absorbing Secondary Organic Aerosols. *ACS Earth Space Chem.* **2018**, *2* (3), 235–245. https://doi.org/10.1021/acsearthspacechem.7b00153.

(19) Kroll, J. H.; Smith, J. D.; Che, D. L.; Kessler, S. H.; Worsnop, D. R.; Wilson, K. R. Measurement of Fragmentation and Functionalization Pathways in the Heterogeneous Oxidation of Oxidized Organic Aerosol. *Phys. Chem. Chem. Phys.* **2009**, *11* (36), 8005. https://doi.org/10.1039/b905289e.

(20) Lee, H. J. (Julie); Aiona, P. K.; Laskin, A.; Laskin, J.; Nizkorodov, S. A. Effect of Solar Radiation on the Optical Properties and Molecular Composition of Laboratory Proxies of Atmospheric Brown Carbon. *Environ. Sci. Technol.* **2014**, *48* (17), 10217–10226. https://doi.org/10.1021/es502515r.

(21) Fleming, L. T.; Lin, P.; Roberts, J. M.; Selimovic, V.; Yokelson, R.; Laskin, J.; Laskin, A.; Nizkorodov, S. A. Molecular Composition and Photochemical Lifetimes of Brown Carbon Chromophores in Biomass Burning Organic Aerosol. *Atmospheric Chemistry and Physics* **2020**, *20* (2), 1105–1129. https://doi.org/10.5194/acp-20-1105-2020.

(22) Zhao, R.; Lee, A. K. Y.; Huang, L.; Li, X.; Yang, F.; Abbatt, J. P. D. Photochemical Processing of Aqueous Atmospheric Brown Carbon. *Atmos. Chem. Phys.* **2015**, *15* (11), 6087–6100. https://doi.org/10.5194/acp-15-6087-2015.

(23) Hems, R. F.; Schnitzler, E. G.; Bastawrous, M.; Soong, R.; Simpson, A. J.; Abbatt, J. P. D. Aqueous Photoreactions of Wood Smoke Brown Carbon. *ACS Earth Space Chem.* **2020**, *4* (7), 1149–1160. https://doi.org/10.1021/acsearthspacechem.0c00117.

(24) Pruppacher, H. R.; Jaenicke, R. The Processing of Water Vapor and Aerosols by Atmospheric Clouds, a Global Estimate. *Atmospheric Research* **1995**, *38* (1), 283–295. https://doi.org/10.1016/0169-8095(94)00098-X.

(25) Walser, M. L.; Park, J.; Gomez, A. L.; Russell, A. R.; Nizkorodov, S. A. Photochemical Aging of Secondary Organic Aerosol Particles Generated from the Oxidation of D-Limonene. *J. Phys. Chem. A* **2007**, *111* (10), 1907–1913. https://doi.org/10.1021/jp066293l.

(26) Mang, S. A.; Henricksen, D. K.; Bateman, A. P.; Andersen, M. P. S.; Blake, D. R.; Nizkorodov, S. A. Contribution of Carbonyl Photochemistry to Aging of Atmospheric Secondary Organic Aerosol. *J. Phys. Chem. A* **2008**, *112* (36), 8337–8344. https://doi.org/10.1021/jp804376c.

(27) Pan, X.; Underwood, J. S.; Xing, J.-H.; Mang, S. A.; Nizkorodov, S. A. Photodegradation of Secondary Organic Aerosol Generated from Limonene Oxidation by Ozone Studied with Chemical Ionization Mass Spectrometry. *Atmospheric Chemistry and Physics* **2009**, *9* (12), 3851–3865. https://doi.org/10.5194/acp-9-3851-2009.

(28) Henry, K. M.; Donahue, N. M. Photochemical Aging of α-Pinene Secondary Organic Aerosol: Effects of OH Radical Sources and Photolysis. *J. Phys. Chem. A* **2012**, *116* (24), 5932–5940. https://doi.org/10.1021/jp210288s.

(29) Malecha, K. T.; Cai, Z.; Nizkorodov, S. A. Photodegradation of Secondary Organic Aerosol Material Quantified with a Quartz Crystal Microbalance. *Environ. Sci. Technol. Lett.* **2018**, *5* (6), 366–371. https://doi.org/10.1021/acs.estlett.8b00231.

(30) Baboomian, V. J.; Gu, Y.; Nizkorodov, S. A. Photodegradation of Secondary Organic Aerosols by Long-Term Exposure to Solar Actinic Radiation. *ACS Earth Space Chem.* **2020**, *4* (7), 1078–1089. https://doi.org/10.1021/acsearthspacechem.0c00088.

(31) Hung, H.-M.; Chen, Y.-Q.; Martin, S. T. Reactive Aging of Films of Secondary Organic Material Studied by Infrared Spectroscopy. *J. Phys. Chem. A* **2013**, *117* (1), 108–116. https://doi.org/10.1021/jp309470z.

(32) Epstein, S. A.; Blair, S. L.; Nizkorodov, S. A. Direct Photolysis of α-Pinene Ozonolysis Secondary Organic Aerosol: Effect on Particle Mass and Peroxide Content. *Environ. Sci. Technol.* **2014**, *48* (19), 11251–11258. https://doi.org/10.1021/es502350u.
(33) Badali, K. M.; Zhou, S.; Aljawhary, D.; Antiñolo, M.; Chen, W. J.; Lok, A.; Mungall, E.; Wong, J. P. S.; Zhao, R.; Abbatt, J. P. D. Formation of Hydroxyl Radicals from Photolysis of Secondary Organic Aerosol Material. *Atmospheric Chemistry and Physics* **2015**, *15* (14), 7831–7840. https://doi.org/10.5194/acp-15-7831-2015.
(34) Krapf, M.; El Haddad, I.; Bruns, E. A.; Molteni, U.; Daellenbach, K. R.; Prévôt, A. S. H.; Baltensperger, U.; Dommen, J. Labile Peroxides in Secondary Organic Aerosol. *Chem* **2016**, *1* (4), 603–616. https://doi.org/10.1016/j.chempr.2016.09.007.
(35) Hinks, M. L.; Brady, M. V.; Lignell, H.; Song, M.; Grayson, J. W.; Bertram, A. K.; Lin, P.; Laskin, A.; Laskin, J.; Nizkorodov, S. A. Effect of Viscosity on Photodegradation Rates in Complex Secondary Organic Aerosol Materials. *Phys. Chem. Chem. Phys.* **2016**, *18* (13), 8785–8793. https://doi.org/10.1039/C5CP05226B.
(36) Dalton, A. B.; Nizkorodov, S. A. Photochemical Degradation of 4-Nitrocatechol and 2,4-Dinitrophenol in a Sugar-Glass Secondary Organic Aerosol Surrogate. *Environ. Sci. Technol.* **2021**, *55* (21), 14586–14594. https://doi.org/10.1021/acs.est.1c04975.
(37) Klodt, A. L.; Adamek, M.; Dibley, M.; Nizkorodov, S. A.; O'Brien, R. E. Effects of the Sample Matrix on the Photobleaching and Photodegradation of Toluene-Derived Secondary Organic Aerosol Compounds. *Atmos. Chem. Phys.* **2022**, *22* (15), 10155–10171. https://doi.org/10.5194/acp-22-10155-2022.
(38) Saleh, R.; Hennigan, C. J.; McMeeking, G. R.; Chuang, W. K.; Robinson, E. S.; Coe, H.; Donahue, N. M.; Robinson, A. L. Absorptivity of Brown Carbon in Fresh and Photo-Chemically Aged Biomass-Burning Emissions. *Atmospheric Chemistry and Physics* **2013**, *13* (15), 7683–7693. https://doi.org/10.5194/acp-13-7683-2013.
(39) Zhong, M.; Jang, M. Dynamic Light Absorption of Biomass-Burning Organic Carbon Photochemically Aged under Natural Sunlight. *Atmospheric Chemistry and Physics* **2014**, *14* (3), 1517–1525. https://doi.org/10.5194/acp-14-1517-2014.
(40) Sumlin, B. J.; Pandey, A.; Walker, M. J.; Pattison, R. S.; Williams, B. J.; Chakrabarty, R. K. Atmospheric Photooxidation Diminishes Light Absorption by Primary Brown Carbon Aerosol from Biomass Burning. *Environ. Sci. Technol. Lett.* **2017**, *4* (12), 540–545. https://doi.org/10.1021/acs.estlett.7b00393.
(41) Calkin, D. E.; Cohen, J. D.; Finney, M. A.; Thompson, M. P. How Risk Management Can Prevent Future Wildfire Disasters in the Wildland-Urban Interface. *Proceedings of the National Academy of Sciences* **2014**, *111* (2), 746–751. https://doi.org/10.1073/pnas.1315088111.
(42) Davis, J. B. The Wildland-Urban Interface: Paradise or Battleground? *Journal of Forestry* **1990**, *88* (1), 26–31.
(43) Radeloff, V. C.; Hammer, R. B.; Stewart, S. I.; Fried, J. S.; Holcomb, S. S.; McKeefry, J. F. The Wildland–Urban Interface in the United States. *Ecological Applications* **2005**, *15* (3), 799–805. https://doi.org/10.1890/04-1413.
(44) Burke, M.; Driscoll, A.; Heft-Neal, S.; Xue, J.; Burney, J.; Wara, M. The Changing Risk and Burden of Wildfire in the United States. *Proceedings of the National Academy of Sciences* **2021**, *118* (2), e2011048118. https://doi.org/10.1073/pnas.2011048118.
(45) Barbero, R.; Abatzoglou, J. T.; Larkin, N. K.; Kolden, C. A.; Stocks, B.; Barbero, R.; Abatzoglou, J. T.; Larkin, N. K.; Kolden, C. A.; Stocks, B. Climate Change Presents Increased

Potential for Very Large Fires in the Contiguous United States. *Int. J. Wildland Fire* **2015**, *24* (7), 892–899. https://doi.org/10.1071/WF15083.
(46) Goss, M.; Swain, D. L.; Abatzoglou, J. T.; Sarhadi, A.; Kolden, C. A.; Williams, A. P.; Diffenbaugh, N. S. Climate Change Is Increasing the Likelihood of Extreme Autumn Wildfire Conditions across California. *Environ. Res. Lett.* **2020**, *15* (9), 094016. https://doi.org/10.1088/1748-9326/ab83a7.
(47) Blomqvist, P.; Persson, B.; McNamee, M. Fire Emissions of Organics into the Atmosphere. *Fire Technology* **2007**, *43*, 213–231. https://doi.org/10.1007/s10694-007-0011-y.
(48) Reisen, F.; Bhujel, M.; Leonard, J. Particle and Volatile Organic Emissions from the Combustion of a Range of Building and Furnishing Materials Using a Cone Calorimeter. *Fire Safety Journal* **2014**, *69*, 76–88. https://doi.org/10.1016/j.firesaf.2014.08.008.
(49) Hewitt, F.; Christou, A.; Dickens, K.; Walker, R.; Stec, A. A. Release of Volatile and Semi-Volatile Toxicants during House Fires. *Chemosphere* **2017**, *173*, 580–593. https://doi.org/10.1016/j.chemosphere.2016.12.079.
(50) Hopstock, K. S.; Carpenter, B. P.; Patterson, J. P.; Al-Abadleh, H. A.; Nizkorodov, S. A. Formation of Insoluble Brown Carbon through Iron-Catalyzed Reaction of Biomass Burning Organics. *Environ. Sci.: Atmos.* **2023**, *3*, 207–220. https://doi.org/10.1039/D2EA00141A.
(51) Devi, M.; Rawat, S.; Sharma, S. A Comprehensive Review of the Pyrolysis Process: From Carbon Nanomaterial Synthesis to Waste Treatment. *Oxford Open Materials Science* **2021**, *1* (1), itab014. https://doi.org/10.1093/oxfmat/itab014.
(52) Santoso, M. A.; Christensen, E. G.; Yang, J.; Rein, G. Review of the Transition From Smouldering to Flaming Combustion in Wildfires. *Front. Mech. Eng.* **2019**, *5*, 49. https://doi.org/10.3389/fmech.2019.00049.
(53) Maldronich, S. *ACOM: Quick TUV calculator, National Center for Atmospheric Research Atmospheric Chemistry Observations and Modeling [code]*. https://www.acom.ucar.edu/Models/TUV/Interactive_TUV/ (accessed 2022-11-03).
(54) Bond, T. C.; Anderson, T. L.; Campbell, D. Calibration and Intercomparison of Filter-Based Measurements of Visible Light Absorption by Aerosols. *Aerosol Science and Technology* **1999**, *30* (6), 582–600. https://doi.org/10.1080/027868299304435.
(55) Lack, D. A.; Cappa, C. D.; Covert, D. S.; Baynard, T.; Massoli, P.; Sierau, B.; Bates, T. S.; Quinn, P. K.; Lovejoy, E. R.; Ravishankara, A. R. Bias in Filter-Based Aerosol Light Absorption Measurements Due to Organic Aerosol Loading: Evidence from Ambient Measurements. *Aerosol Science and Technology* **2008**, *42* (12), 1033–1041. https://doi.org/10.1080/02786820802389277.
(56) O'Brien, R. E.; Kroll, J. H. Photolytic Aging of Secondary Organic Aerosol: Evidence for a Substantial Photo-Recalcitrant Fraction. *J. Phys. Chem. Lett.* **2019**, *10* (14), 4003–4009. https://doi.org/10.1021/acs.jpclett.9b01417.
(57) West, C. P.; Hsu, Y.-J.; MacFeely, K. T.; Huston, S. M.; Aridjis-Olivos, B. P.; Morales, A. C.; Laskin, A. Volatility Measurements of Individual Components in Organic Aerosol Mixtures Using Temperature-Programmed Desorption–Direct Analysis in Real Time–High Resolution Mass Spectrometry. *Anal. Chem.* **2023**. https://doi.org/10.1021/acs.analchem.3c00923.
(58) Roach, P. J.; Laskin, J.; Laskin, A. Higher-Order Mass Defect Analysis for Mass Spectra of Complex Organic Mixtures. *Anal. Chem.* **2011**, *83* (12), 4924–4929. https://doi.org/10.1021/ac200654j.

(59) Blomqvist, P.; McNamee, M. S.; Stec, A. A.; Gylestam, D.; Karlsson, D. Detailed Study of Distribution Patterns of Polycyclic Aromatic Hydrocarbons and Isocyanates under Different Fire Conditions. *Fire and Materials* **2014**, *38* (1), 125–144. https://doi.org/10.1002/fam.2173.
(60) Xu, Z.; Feng, W.; Wang, Y.; Ye, H.; Wang, Y.; Liao, H.; Xie, M. Potential Underestimation of Ambient Brown Carbon Absorption Based on the Methanol Extraction Method and Its Impacts on Source Analysis. *Atmos. Chem. Phys.* **2022**, *22* (20), 13739–13752. https://doi.org/10.5194/acp-22-13739-2022.
(61) Sengupta, D.; Samburova, V.; Bhattarai, C.; Kirillova, E.; Mazzoleni, L.; Iaukea-Lum, M.; Watts, A.; Moosmüller, H.; Khlystov, A. Light Absorption by Polar and Non-Polar Aerosol Compounds from Laboratory Biomass Combustion. *Atmos. Chem. Phys.* **2018**, *18* (15), 10849–10867. https://doi.org/10.5194/acp-18-10849-2018.
(62) Saleh, R. From Measurements to Models: Toward Accurate Representation of Brown Carbon in Climate Calculations. *Curr Pollution Rep* **2020**, *6* (2), 90–104. https://doi.org/10.1007/s40726-020-00139-3.
(63) Moise, T.; Flores, J. M.; Rudich, Y. Optical Properties of Secondary Organic Aerosols and Their Changes by Chemical Processes. *Chem. Rev.* **2015**, *115* (10), 4400–4439. https://doi.org/10.1021/cr5005259.
(64) Chin, H.; S. Hopstock, K.; T. Fleming, L.; A. Nizkorodov, S.; A. Al-Abadleh, H. Effect of Aromatic Ring Substituents on the Ability of Catechol to Produce Brown Carbon in Iron(Iii)-Catalyzed Reactions. *Environmental Science: Atmospheres* **2021**, *1* (2), 64–78. https://doi.org/10.1039/D0EA00007H.
(65) Schwarzenbach, R. P.; Gschwend, P. M.; Imboden, D. M. *Environmental Organic Chemistry*, 2. ed.; Wiley-Interscience; Wiley: New York, 2003.
(66) Leskinen, J.; Tissari, J.; Uski, O.; Virén, A.; Torvela, T.; Kaivosoja, T.; Lamberg, H.; Nuutinen, I.; Kettunen, T.; Joutsensaari, J.; Jalava, P. I.; Sippula, O.; Hirvonen, M.-R.; Jokiniemi, J. Fine Particle Emissions in Three Different Combustion Conditions of a Wood Chip-Fired Appliance – Particulate Physico-Chemical Properties and Induced Cell Death. *Atmospheric Environment* **2014**, *86*, 129–139. https://doi.org/10.1016/j.atmosenv.2013.12.012.
(67) Molchanov, O.; Krpec, K.; Horák, J.; Kuboňová, L.; Hopan, F. Comparison of Methods for Evaluating Particle Charges in the Electrostatic Precipitation of Fly-Ash from Small-Scale Solid Fuel Combustion. *Separation and Purification Technology* **2020**, *248*, 117057. https://doi.org/10.1016/j.seppur.2020.117057.
(68) Ye, Z.; Qu, Z.; Ma, S.; Luo, S.; Chen, Y.; Chen, H.; Chen, Y.; Zhao, Z.; Chen, M.; Ge, X. A Comprehensive Investigation of Aqueous-Phase Photochemical Oxidation of 4-Ethylphenol. *Science of The Total Environment* **2019**, *685*, 976–985. https://doi.org/10.1016/j.scitotenv.2019.06.276.
(69) Cai, J.; Zeng, X.; Zhi, G.; Gligorovski, S.; Sheng, G.; Yu, Z.; Wang, X.; Peng, P. Molecular Composition and Photochemical Evolution of Water-Soluble Organic Carbon (WSOC) Extracted from Field Biomass Burning Aerosols Using High-Resolution Mass Spectrometry. *Atmospheric Chemistry and Physics* **2020**, *20* (10), 6115–6128. https://doi.org/10.5194/acp-20-6115-2020.
(70) Mekic, M.; Liu, J.; Zhou, W.; Loisel, G.; Cai, J.; He, T.; Jiang, B.; Yu, Z.; Lazarou, Y. G.; Li, X.; Brigante, M.; Vione, D.; Gligorovski, S. Formation of Highly Oxygenated Multifunctional Compounds from Cross-Reactions of Carbonyl Compounds in the

Atmospheric Aqueous Phase. *Atmospheric Environment* **2019**, *219*, 117046. https://doi.org/10.1016/j.atmosenv.2019.117046.
(71) Mu, Z.; Chen, Q.; Zhang, L.; Guan, D.; Li, H. Photodegradation of Atmospheric Chromophores: Changes in Oxidation State and Photochemical Reactivity. *Atmospheric Chemistry and Physics* **2021**, *21* (15), 11581–11591. https://doi.org/10.5194/acp-21-11581-2021.
(72) Jiang, W.; Misovich, M. V.; Hettiyadura, A. P. S.; Laskin, A.; McFall, A. S.; Anastasio, C.; Zhang, Q. Photosensitized Reactions of a Phenolic Carbonyl from Wood Combustion in the Aqueous Phase—Chemical Evolution and Light Absorption Properties of AqSOA. *Environ. Sci. Technol.* **2021**, *55* (8), 5199–5211. https://doi.org/10.1021/acs.est.0c07581.
(73) Hems, R. F.; Abbatt, J. P. D. Aqueous Phase Photo-Oxidation of Brown Carbon Nitrophenols: Reaction Kinetics, Mechanism, and Evolution of Light Absorption. *ACS Earth Space Chem.* **2018**, *2* (3), 225–234. https://doi.org/10.1021/acsearthspacechem.7b00123.
(74) Sareen, N.; Moussa, S. G.; McNeill, V. F. Photochemical Aging of Light-Absorbing Secondary Organic Aerosol Material. *J. Phys. Chem. A* **2013**, *117* (14), 2987–2996. https://doi.org/10.1021/jp309413j.
(75) Ye, Z.; Zhuang, Y.; Chen, Y.; Zhao, Z.; Ma, S.; Huang, H.; Chen, Y.; Ge, X. Aqueous-Phase Oxidation of Three Phenolic Compounds by Hydroxyl Radical: Insight into Secondary Organic Aerosol Formation Yields, Mechanisms, Products and Optical Properties. *Atmospheric Environment* **2020**, *223*, 117240. https://doi.org/10.1016/j.atmosenv.2019.117240.
(76) Hettiyadura, A. P. S.; Garcia, V.; Li, C.; West, C. P.; Tomlin, J.; He, Q.; Rudich, Y.; Laskin, A. Chemical Composition and Molecular-Specific Optical Properties of Atmospheric Brown Carbon Associated with Biomass Burning. *Environ. Sci. Technol.* **2021**, *55* (4), 2511–2521. https://doi.org/10.1021/acs.est.0c05883.
(77) Ren, B.-Z.; Hou, C.-H.; Chong, H.-G.; Li, W.-R.; Song, H.-J. Solubility of O-Phthalic Acid in Methanol + Water and Methanol + Butyl Acetate from (295.87 to 359.75) K. *J. Chem. Eng. Data* **2006**, *51* (6), 2022–2025. https://doi.org/10.1021/je0600505.
(78) Cain, J.; Laskin, A.; Kholghy, M. R.; Thomson, M. J.; Wang, H. Molecular Characterization of Organic Content of Soot along the Centerline of a Coflow Diffusion Flame. *Phys. Chem. Chem. Phys.* **2014**, *16* (47), 25862–25875. https://doi.org/10.1039/C4CP03330B.
(79) Lin, P.; Fleming, L. T.; Nizkorodov, S. A.; Laskin, J.; Laskin, A. Comprehensive Molecular Characterization of Atmospheric Brown Carbon by High Resolution Mass Spectrometry with Electrospray and Atmospheric Pressure Photoionization. *Anal. Chem.* **2018**, *90* (21), 12493–12502. https://doi.org/10.1021/acs.analchem.8b02177.
(80) G. Schnitzler, E.; Liu, T.; F. Hems, R.; D. Abbatt, J. P. Emerging Investigator Series: Heterogeneous OH Oxidation of Primary Brown Carbon Aerosol: Effects of Relative Humidity and Volatility. *Environmental Science: Processes & Impacts* **2020**, *22* (11), 2162–2171. https://doi.org/10.1039/D0EM00311E.
(81) Yu, L.; Smith, J.; Laskin, A.; Anastasio, C.; Laskin, J.; Zhang, Q. Chemical Characterization of SOA Formed from Aqueous-Phase Reactions of Phenols with the Triplet Excited State of Carbonyl and Hydroxyl Radical. *Atmospheric Chemistry and Physics* **2014**, *14* (24), 13801–13816. https://doi.org/10.5194/acp-14-13801-2014.